

12-21-2017

Silver Photodiffusion into Ge-Rich Amorphous Germanium Sulfide—Neutron Reflectivity Study

Y. Sakaguchi

Comprehensive Research Organization for Science and Society

H. Asaoka

Japan Atomic Energy Agency

M. Mitkova

Boise State University

Copyright (2017) American Institute of Physics. This article may be downloaded for personal use only. Any other use requires prior permission of the author and the American Institute of Physics. The following article appeared in:

Sakaguchi, Y.; Asaoka, H.; & Mitkova M. (2017). Silver photodiffusion into Ge-rich amorphous germanium sulfide-neutron reflectivity study. *Journal of Applied Physics*, 122(23), 235105.

and may be found at doi: [10.1063/1.5000858](https://doi.org/10.1063/1.5000858)

Silver photodiffusion into Ge-rich amorphous germanium sulfide—neutron reflectivity study

Y. Sakaguchi,^{1,a)} H. Asaoka,² and M. Mitkova³

¹Neutron Science and Technology Center, Comprehensive Research Organization for Science and Society (CROSS), Tokai 319-1106, Japan

²Advanced Science Research Center, Japan Atomic Energy Agency (JAEA), Tokai 319-1195, Japan

³Department of Electrical and Computer Engineering, Boise State University (BSU), 1910 University Dr. Boise, Idaho 83725-2075, USA

(Received 18 August 2017; accepted 30 November 2017; published online 21 December 2017)

Silver diffuses into chalcogenide films upon light exposure, and the kinetics of photodiffusion has been a subject of various investigations because of the difficulties in the *in situ* determination of the time-dependent Ag reaction and diffusion development in the chalcogenide layers. In this paper, we report the results of time-resolved neutron reflectivity measurement of Ag/Ge₄₀S₆₀/Si substrates under light exposure to clarify the kinetics of Ag photodiffusion into Ge-rich Ge chalcogenides. It reveals that Ag ions diffuse all over the Ge chalcogenide host layer once Ag dissolves into the layer without forming a metastable reaction layer unlike the case of S-rich Ge chalcogenide such as Ge₂₀S₈₀. The decay curve suggests that the Ag dissolution is determined by two types of Ag capturing chalcogen sites. Also, the observed relaxation time showed anomalous chalcogenide layer thickness dependence. This is attributed to an additional diffusion-driven accelerating factor, which is unique to the silver photodiffusion. Furthermore, we observed indicative changes in the formation of an inhomogeneous in-plane structure at the Ag/chalcogenide interface. This would be related to the nucleation and growth of the Ag-dissolved reaction product. *Published by AIP Publishing.*

<https://doi.org/10.1063/1.5000858>

I. INTRODUCTION

Amorphous chalcogenides exhibit various photo-induced changes due to their structural flexibility.¹ Silver photodiffusion^{2,3} is one of them, and it has been attracting much attention from fundamental and application points of view since its discovery in 1966.² This phenomenon occurs because of the excitation of lone-pair electrons related to chalcogen atoms and Ag ionization by light. Electrons, ions, and structural stability are closely related to each other for its manifestation, and an interdisciplinary approach between amorphous semiconductor physics and ion conductor physics is required to understand the photo-induced Ag diffusion into chalcogenide glasses. There are potential applications such as photoresist,⁴ the fabrication of relief images in optical elements,⁵ optical waveguides, microgratings, holographic gratings,⁶ and non-volatile memory devices,⁷ and the understanding of the mechanism is also of interest for the application field. So far, there have been considerable investigations on the kinetics of silver photodiffusion. Many different studies have been utilized to give information about how Ag ions diffuse into the chalcogenide (Ch) layer—from electrical resistivity measurement,^{8,9} optical transmittance measurement,¹⁰ modified optical reflectivity measurement,^{11–13} X-ray diffraction measurement,^{14,15} to Rutherford backscattering (RBS).^{16–22} Among these techniques, electrical resistivity and X-ray diffraction are good tools to evaluate the Ag thickness, but it is difficult to obtain information on the chalcogenide layer and the reaction layer through them. The optical transmittance

and reflection measurements are also good techniques to find the time-dependent change in the selected layer. However, it is also difficult to provide information on all layers. RBS is the powerful technique to clarify the depth profile of all compositional elements. From several RBS works, it was demonstrated that photo-diffused films showed a step-like silver distribution, in which Ag concentration was constant in the reaction layer in the depth direction, but it abruptly dropped at a certain point.

Ideally speaking, it would be best to perform *in situ* RBS to clarify the silver diffusion kinetics, in which the position of Ag ions in the depth direction is definitely demonstrated. However, the *in situ* RBS would give incorrect results, because the strong ion beam used should also induce silver diffusion.^{17,18,21,23} Therefore, precise RBS studies on silver diffusion kinetics have been done by *ex situ* techniques, using weak ion beams and several films with different illumination times. However, it is desirable to perform *in situ* studies using a proper probe beam.

X-ray/neutron reflectivity is also a powerful technique to clarify the depth profiles in multi-layer films. The use of brilliant X-ray beams such as synchrotron radiation will provide precise information on the time-dependent change. However, silver diffusion can also be induced by a strong X-ray beam,²⁴ and the use of neutron beams is considered safer. Recently, we performed neutron reflectivity measurements of Ag/Ge chalcogenide films^{25–29} and found that this technique is quite useful to observe the time-dependent changes in the films in the depth direction without inducing the silver diffusion by the probe beam itself. From the preliminary results of the Ag/Ge₂₀S₈₀/Si substrate, the Ag/Ge₂₅S₇₅/Si substrate, and the

^{a)}Electronic mail: y_sakaguchi@cross.or.jp

Ag/Ge₄₀S₆₀/Si substrate,^{25,28} it was found that silver diffusion kinetics markedly depends on Ge composition. A detailed measurement and analysis of the stoichiometric composition, Ge₃₃S₆₇/Ag/Si substrates, revealed the time variation of the thicknesses of Ag and the reaction layers, and a clear Ch layer thickness dependence on the silver diffusion was found from the study.²⁹ In this paper, we focus on a Ge-rich compound, which is considered to show different behavior from the stoichiometric composition, and report the detailed results of neutron reflectivity measurements of Ag/Ge₄₀S₆₀/Si substrate films. In addition, we discuss the mechanism of silver photo-diffusion into the Ge-rich compound layer, based on the experimental result.

II. EXPERIMENTAL

Neutron reflectivity is theoretically calculated by giving the scattering length density (SLD), the thickness, the roughness, and the modulus of the wavevector transfer Q , using Parratt's recursive method or the Abeles matrix method.^{30–32} The SLD is given by $\sum_i n_i(z)b_i$, where n_i is the number density (L^{-3}) of the i -th nucleus at the distance of z from the interface and b_i is the scattering length of the nucleus. Usually, the experimental reflectivity is evaluated by comparing it with the calculated one from a SLD depth profile model. Recently, Fourier transform technique was suggested as a model-free analysis to clarify a basic multi-layer structure of films in terms of the number of layers and their thicknesses.^{33,34} Since it was not easy to assume a proper model in the present study, we performed Fourier transform analysis before performing a model calculation. The neutron reflectivity measurements were carried out on a SHARAKU (BL17)³⁵ at the Materials and Life Science Experimental Facility (MLF) of the Japan Proton Accelerator Research Complex (J-PARC). At the MLF, intense pulsed neutrons are generated through nuclear spallation reactions between a high-energy proton beam and the liquid-Hg target with a repetition rate of 25 Hz. The neutron flux is proportional to the power of the incident proton beam which was about 200 kW in the experiment. White light from a 300 W xenon lamp (MAX-303, ASAHI Spectra, Co., Ltd.) was used as an excitation light source. Using a mirror module for the visible light region, the light has a spectrum in the range from 350 to 800 nm (the mirror module has the transmittance more than 90% from 390 to 720 nm). Neutron reflectivity, R , was obtained by $R = I/I_0$, where I is the intensity of the reflected beam and I_0 is the intensity of the incident beam as a function of neutron time-of-flight (TOF), t_{TOF} . I_0 was obtained by measuring the intensity of the direct beam without a sample. The TOF was converted to Q , using the relationships: $\lambda = ht_{TOF}/mL$, where λ is the neutron wavelength, h is Planck's constant, m is the mass of a neutron, and L is the length between the neutron source and the detector, and $Q = 4\pi \sin \theta/\lambda$ where $\theta = \theta_i$ (incident angle) = θ_f (scattering angle). Static measurements before and after light exposure were performed by fixing at two different angles, 0.4° and 0.8°. Transient measurement during light exposure was performed by fixing at one angle, 0.4°, and the time evolution of the transient TOF spectrum was measured using an

event-data recording system. Using the data reduction system, arbitrarily time sliced spectra can be obtained from the recorded data. In the measurement, the collimation slits for the incident beam were set to be $\Delta\theta/\theta = 3\%$. The details of the experimental procedure are shown elsewhere.²⁷ The obtained neutron reflectivity profiles were fitted using the Motofit package.³⁶

X-ray diffraction was measured using a RINT-Ultima-III (Rigaku) with an asymmetric diffraction geometry fixing the incident angle at 0.5° using a Cu K_α incident beam (0.15418 nm). X-ray reflectivity was measured using a ATX-G (Rigaku) with a Cu K_α incident beam (0.15405 nm) using a two-crystal (Ge(220)) monochromator.

A bulk Ge₄₀S₆₀ glass was prepared from high purity Ge and S by using the traditional melt quenching technique. The glass was then thermally deposited onto a silicon wafer from a semi-Knudsen cell crucible in an attempt to keep the composition of the film identical with that of the source material. The deposition process was carried out in a Cressington 308R evaporation system at a pressure of 1×10^{-6} mbar. The thickness of the deposited films was monitored during the evaporation process using a quartz monitor which was mounted very close to the silicon wafer on which the films were deposited. The wafer was rotated during the deposition for equilibration of the composition and the thickness of the films. The chalcogenide glass films were either 150 nm or 200 nm thick, and their deposition rate was about 0.1 nm/s. On top of these films was deposited a 50 nm Ag film at a deposition rate of 0.2 nm/s, and the so-prepared bi-layer units were further studied by neutron reflectivity.

III. RESULTS AND DISCUSSION

A. Neutron reflectivity measurement

1. Neutron reflectivity before and after light exposure—accumulated total light effect

Static neutron reflectivity profiles of a Ag 50 nm/Ge₄₀S₆₀ 150 nm/Si substrate before and after 117 min of light exposure and a Ag 50 nm/Ge₄₀S₆₀ 200 nm/Si substrate before and after 94 min of light exposure are shown in Fig. 1. Fourier transforms of RQ^4 are shown in Fig. 2. The position of the peak indicates the thickness of the layer in the film. In the Fourier transform of the Ag 50 nm/Ge₄₀S₆₀ 150 nm/Si substrate before the light exposure, there are three peaks at 42, 123, and 165 nm, showing the layer thickness of Ag, Ge₄₀S₆₀ and the sum of these layers, respectively. In general, ${}_{n+1}C_2 = (n+1)n/2$ peaks (C : combination, ${}_nC_r = n!/\{r!(n-r)!\}$) are observed in the Fourier transform, for a multi-layer thin film composed of n layers, which have $(n+1)$ interfaces.³⁴ The results of the number of peaks and their positions ensure that the two-layer structure composed of Ag and Ge₄₀S₆₀ layers is intact without any reaction during the measurement before the light exposure and that the film was prepared with roughly the same thicknesses as we have controlled by a crystal monitor during thermal evaporation. After 117 min of light exposure, there are still three peaks, and the position shifted to 40, 130, and 170 nm, respectively. This means that the

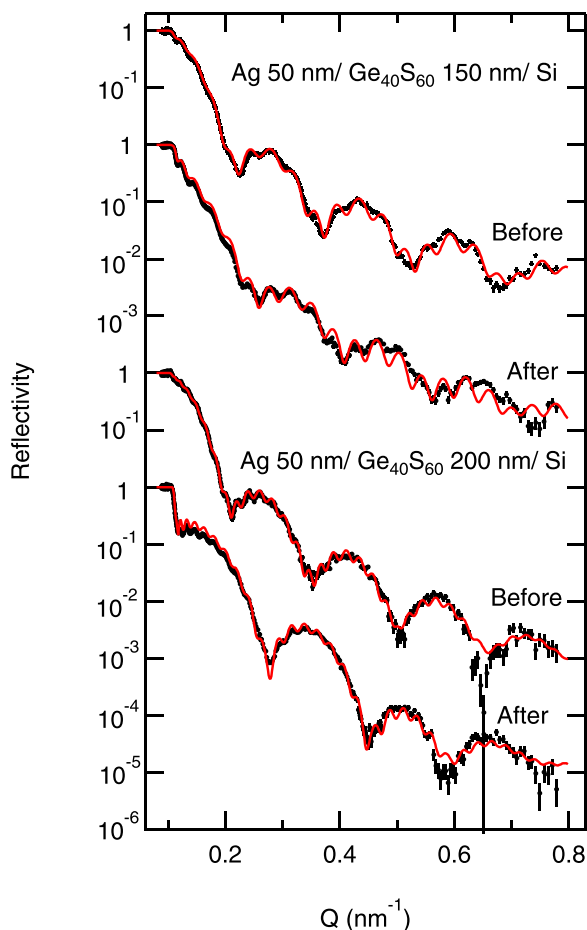


FIG. 1. Static neutron reflectivity profiles of the Ag 50 nm/Ge₄₀S₆₀ 150 nm/Si substrate and the Ag 50 nm/Ge₄₀S₆₀ 200 nm/Si substrate before and after light exposure (dots with error bars) and the calculated curves by model fitting (red curves). The curves are shifted vertically for readability.

two-layer structure is maintained after the light exposure. In our previous paper,²⁵ we interpreted that Ag/Ge₄₀S₆₀ changed to two reaction layers with different Ag content after the light exposure. However, the results of X-ray diffraction measurements suggest that the Ag layer still exists in the sample after the light exposure (see, Appendix A). Therefore, the shift of the peak position indicates that the Ag layer becomes thinner from 42 to 40 nm and the Ch layer expands from 123 to 130 nm upon the introduction of Ag ions. For the Ag 50 nm/Ge₄₀S₆₀ 200 nm/Si substrate, the first peak shifts from 45 nm to 36.5 nm upon light exposure. This indicates that Ag is more dissolved in Ag 50 nm/Ge₄₀S₆₀ 200 nm/Si.

Considering the results of the Fourier transform and the X-ray diffraction, we performed a model fitting to the neutron reflectivity curve, and the result is shown in Fig. 3. The fitted curves are shown as red curves in Fig. 1. It is noted that a metastable Ag-rich reaction layer is not formed between the Ag layer and the Ch layer, and that one uniform reaction layer is formed throughout the Ch host layer. This means that the Ag ions immediately diffuse all over the Ch host layer once they dissolve into the Ch host layer upon light exposure. This diffusion process is the same as that of the stoichiometric Ge₃₃S₆₇/Ag/Si substrate,²⁹ and is in contrast to the S-rich case of Ag/Ge₂₀S₈₀ (Ref. 25) and Ag/Ge₂₅S₇₅.²⁸ Considering the residual amount of the Ag layer after light exposure for

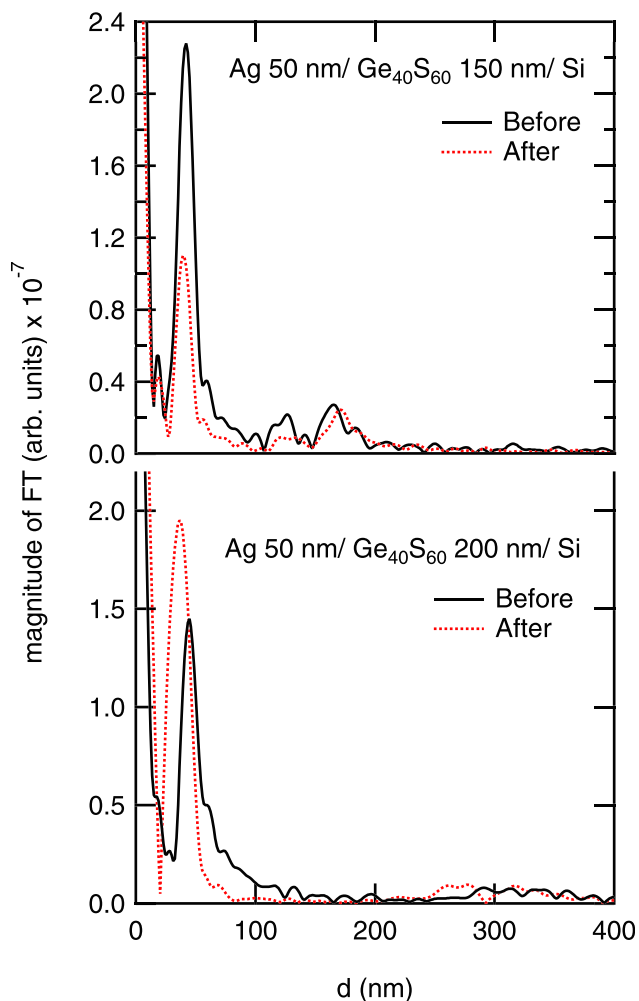


FIG. 2. Fourier transforms of RQ^4 of the Ag 50 nm/Ge₄₀S₆₀ 150 nm/Si substrate and the Ag 50 nm/Ge₄₀S₆₀ 200 nm/Si substrate before and after light exposure.

the samples with different Ge-compositions and the previous studies of Ag diffusion in S-rich films,³⁷ it seems that more sulfur content leads to more silver dissolution into the Ch layer. We assume the reason to be not only the leading role of the electron-hole pair formation in the chalcogen atoms and Ag ionization by light illumination but also the difference in diffusion products that form.³⁸ This specificity of the diffusion phenomenon is obviously related to the dual role of Ag as a dopant in the Ge-chalcogenide systems.³⁹ The Ag-doped reaction layer is supposed to be in an amorphous form as our previous X-ray diffraction measurements suggest.⁴⁰

It is also noted that there is a dip in the SLD profile between the Ag layer and the Ch host layer after the light exposure. Especially, the dip is very deep in the Ag 50 nm/Ge₄₀S₆₀ 200 nm/Si substrate. Such a dip was needed to fit the neutron reflectivity curve. Although the model may not be the unique solution for the curve fitting, the dip was also observed in the SLD profile obtained from X-ray reflectivity measurements (see, Appendix B), and the presence of the dip is supposed to be probable. The presence of the dip can also be explained from the result of Fourier transform in Fig. 2. According to the theory of the Fourier transform of X-ray/neutron reflectivity,³² the reflectivity, R , is expressed as

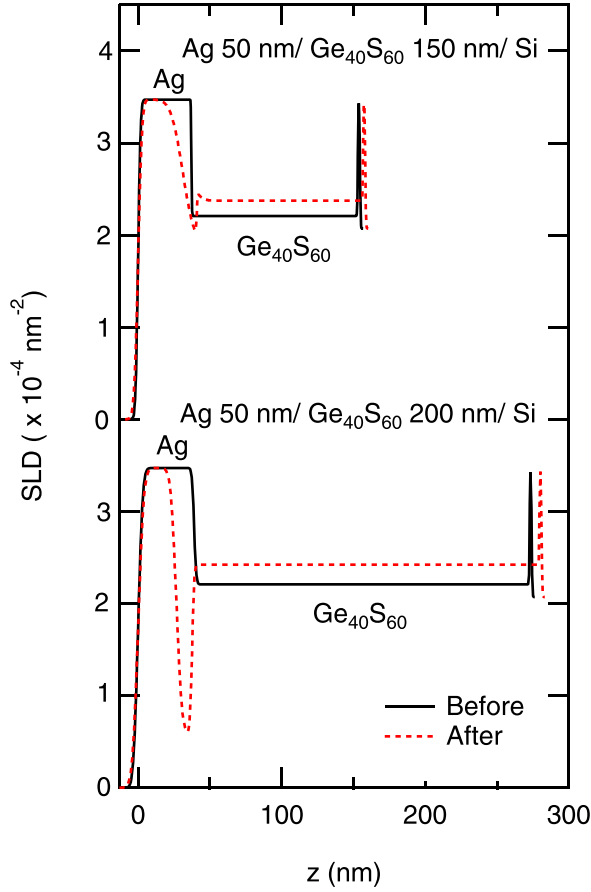


FIG. 3. SLD profiles of the Ag 50 nm/Ge₄₀S₆₀ 150 nm/Si substrate and the Ag 50 nm/Ge₄₀S₆₀ 200 nm/Si substrate before (black solid line) and after light exposure (red broken line).

$$R(Q) \approx \frac{16\pi^2}{Q^4} \left| \int_{-\infty}^{\infty} \frac{d\beta}{dz} e^{-izQ} dz \right|^2. \quad (1)$$

When we consider the simple case of one uniform layer, of thickness L and SLD β_1 , on a substrate of SLD β_s , the depth profile of the SLD is given by

$$\beta(z) = \begin{cases} \beta_s & z < -L \\ \beta_1 & -L < z < 0 \\ \beta_{air} = 0 & z > 0, \end{cases} \quad (2)$$

and the reflectivity is expressed as

$$R(Q) \approx \frac{16\pi^2}{Q^4} \left[(\beta_s - \beta_1)^2 + (\beta_1 - \beta_{air})^2 + 2(\beta_s - \beta_1)(\beta_1 - \beta_{air}) \cos(LQ) \right]. \quad (3)$$

Overall, we will find a peak at L by the Fourier transform of RQ^4 , and the height of the peak should be proportional to the amplitude of the cosine curve in Eq. (3). It is noted that the amplitude of the cosine curve is expressed as the product of the differences (the contrast) in the SLD at two interfaces. This means that the height of the first peak in Fig. 2 is related to the product of the contrast at both interfaces of the Ag layer (air side and Ch side). As far as the Ag layer remains in the Ag dissolution process, the contrast at

the air/Ag interface does not change and we can only consider the change in the contrast at the Ag/Ch interface. In Fig. 2, the first peak height decreases upon light exposure in the Ag 50 nm/Ge₄₀S₆₀ 150 nm/Si substrate, while it increases in the Ag 50 nm/Ge₄₀S₆₀ 200 nm/Si substrate. This means that the contrast at the Ag/Ch interface decreases in the Ag 50 nm/Ge₄₀S₆₀ 150 nm/Si substrate, while it increases in the Ag 50 nm/Ge₄₀S₆₀ 200 nm/Si substrate. In fact, the SLD profiles in Fig. 3 are consistent with the expectation; the contrast decreases on average in the Ag 50 nm/Ge₄₀S₆₀ 150 nm/Si substrate, considering the small depth of the dip and the large roughness at the interface, while the contrast increases in the Ag 50 nm/Ge₄₀S₆₀ 200 nm/Si substrate by assuming the deep dip between the Ag layer and the Ch layer. The physical origin of the dip will be discussed later.

Finally, we would like to remark on the effect of the neutron beam on the silver diffusion. The sample was exposed to the neutron beam before the light exposure for 7 h to obtain the neutron reflectivity of the Ag 50 nm/Ge₄₀S₆₀ 150 nm/Si substrate and for 3 h to obtain the neutron reflectivity of the Ag 50 nm/Ge₄₀S₆₀ 200 nm/Si substrate. During the measurement, there was no time-dependent change in the spectrum. Also, the result of the model fitting assured that the films

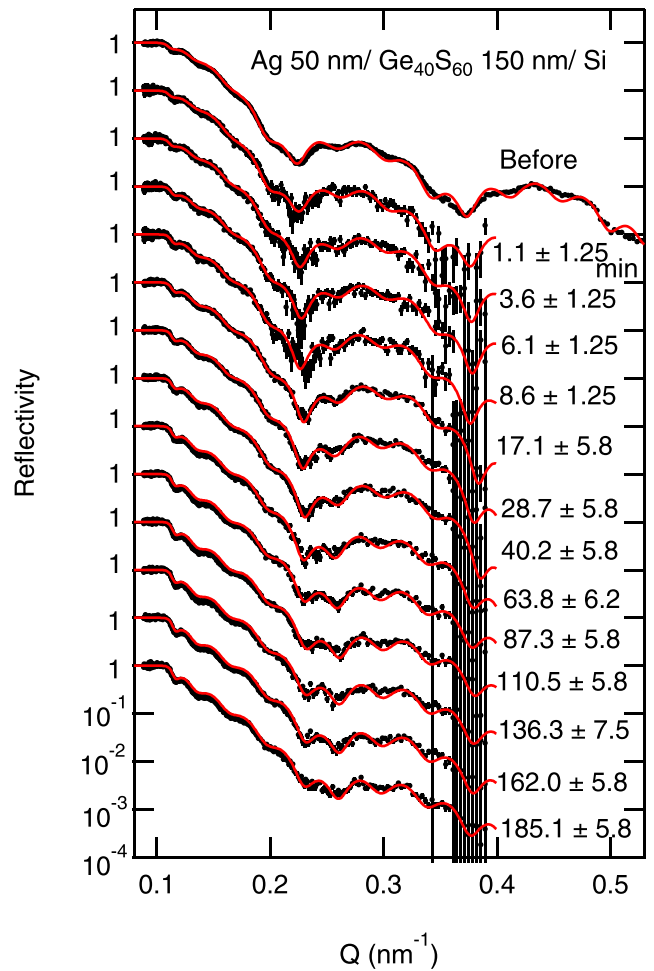


FIG. 4. Time evolution of neutron reflectivity profiles of the Ag 50 nm/Ge₄₀S₆₀ 150 nm/Si substrate during and after light exposure for 117 min. The calculated neutron reflectivity profiles by model fitting are indicated by red curves. The curves are shifted vertically for readability.

were intact by neutron beam irradiation. The result strongly supports that the neutron beam is a good probe to perform *in situ* measurements.

2. Time-resolved neutron reflectivity—photodiffusion kinetics

The time evolution of neutron reflectivity profiles during and after light exposure is shown in Fig. 4 (Ag 50 nm/Ge₄₀S₆₀ 150 nm/Si substrate) and Fig. 5 (Ag 50 nm/Ge₄₀S₆₀ 200 nm/Si substrate). Although the Q range was limited to $0.09 < Q < 0.40 \text{ nm}^{-1}$, the range is considered enough as the analytical result shown later will demonstrate. The time width of the transient spectrum was determined, considering the speed of the photo-induced changes and the statistics of the data.

Fourier transform of RQ^4 is shown in Fig. 6 (Ag 50 nm/Ge₄₀S₆₀ 150 nm/Si substrate) and in Fig. 7 (Ag 50 nm/Ge₄₀S₆₀ 200 nm/Si substrate). In both cases, the first peak shifts to the thinner side upon light exposure, but it still remains in the observable thickness range during the light exposure time. This indicates that the Ag layer becomes thinner by silver photodiffusion, but the Ag layer remains even after the light exposure in both cases.

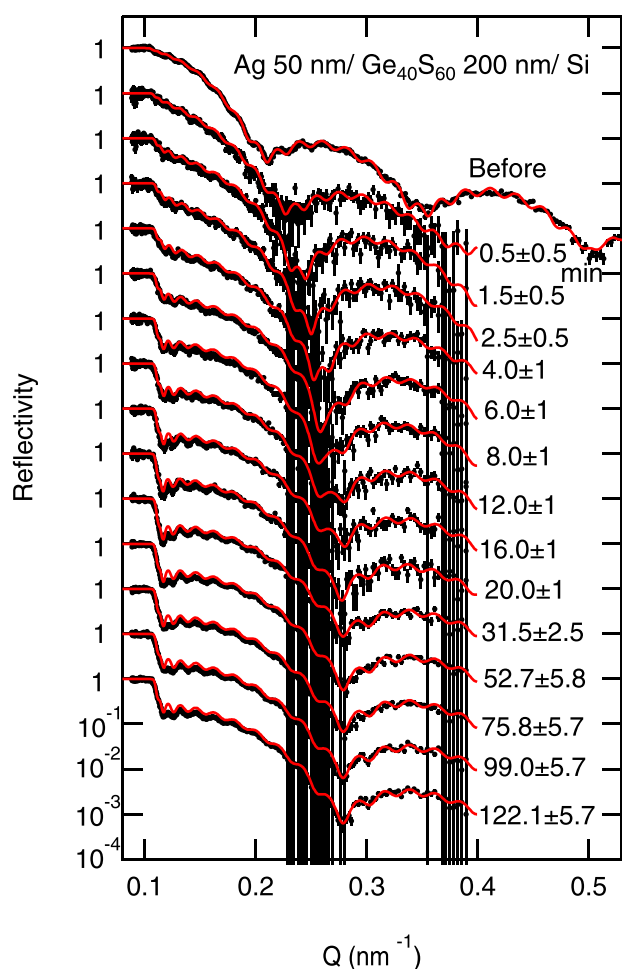


FIG. 5. Time evolution of neutron reflectivity profiles of the Ag 50 nm/Ge₄₀S₆₀ 200 nm/Si substrate during and after light exposure for 94 min. The calculated neutron reflectivity profiles by model fitting are indicated by red curves. The curves are shifted vertically for readability.

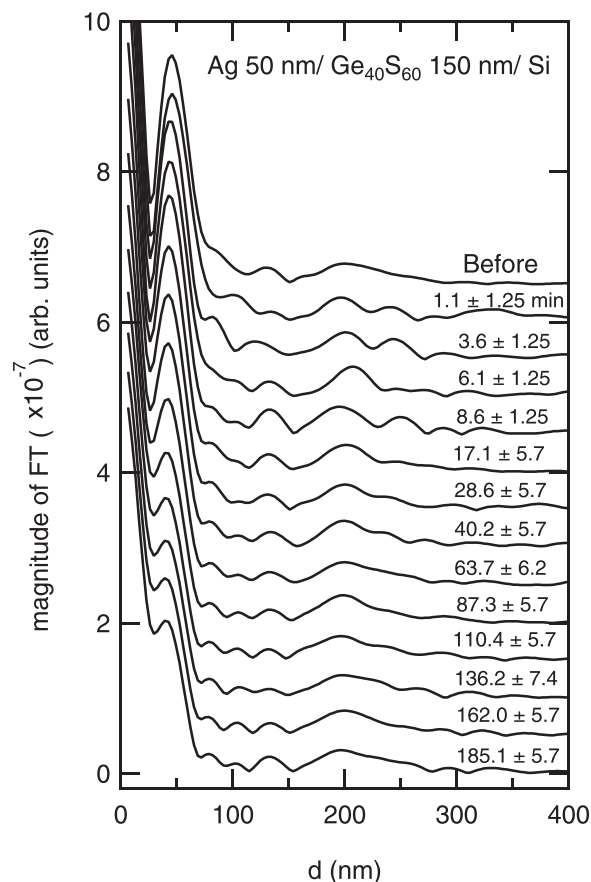


FIG. 6. Time evolution of the Fourier transform of RQ^4 of the Ag 50 nm/Ge₄₀S₆₀ 150 nm/Si substrate during light exposure. The curves are shifted vertically for readability.

Time variation of the position and the height of the first peak in the Fourier transform is shown in Fig. 8. For the Ag 50 nm/Ge₄₀S₆₀ 200 nm/Si substrate, the peak position decreases from 47 to 32 nm, suggesting the decrease of the Ag thickness by 15 nm by silver photodiffusion. It decreases rapidly in the first 2 min and continues to decrease in the next 20 min, reaching a saturation. For the Ag 50 nm/Ge₄₀S₆₀ 150 nm/Si substrate, the peak position rapidly decreases in the first 10 min by 3 nm, and then, gradually decreases until the light shutter is closed. The peak position changes from 47 to 40 nm by 7 nm, in total. It seems that there are two reaction stages with different relaxation times for both the films. As for the peak height, it rapidly increases in the first 20 min, and then decreases after 20 min for the Ag 50 nm/Ge₄₀S₆₀ 200 nm/Si substrate, while it moderately increases in the first 10 min, and then, decreases after 10 min for the Ag 50 nm/Ge₄₀S₆₀ 150 nm/Si substrate. Considering the relationship between the first peak height and the difference in the SLD at the Ag/Ch interface, the decrease of the peak height of the Ag 50 nm/Ge₄₀S₆₀ 150 nm/Si substrate, which is observed after 10 min, indicates the silver diffusion because the difference in the SLD decreases by the introduction of Ag ions into the Ch host layer. On the other hand, the increase of the peak height of the Ag 50 nm/Ge₄₀S₆₀ 200 nm/Si substrate, which is observed in the first 20 min, indicates the appearance of the interface layer with a smaller SLD than the Ch host layer because the difference in the SLD increases by the growth of such an interface layer. Since the maximum peak height is

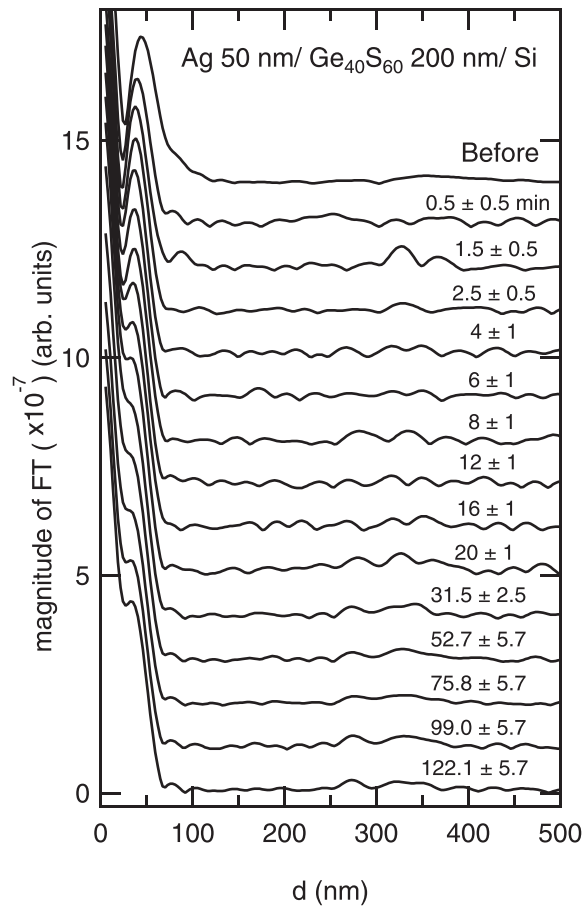


FIG. 7. Time evolution of the Fourier transform of RQ^4 of the Ag 50 nm/ $\text{Ge}_{40}\text{S}_{60}$ 200 nm/Si substrate during light exposure. The curves are shifted vertically for readability.

about 1.7 times of the initial one, the SLD of the interface layer is supposed to be very small.

Assuming that the above changes are expected from the result of the Fourier transform, we performed a model fitting to the experimental neutron reflectivity profile. The time evolution of the obtained SLD profile model is shown in Fig. 9 (Ag 50 nm/ $\text{Ge}_{40}\text{S}_{60}$ 150 nm/Si substrate) and Fig. 10 (Ag 50 nm/ $\text{Ge}_{40}\text{S}_{60}$ 200 nm/Si substrate). The fitted reflectivity profiles are shown as red curves in Figs. 4 and 5. The time evolution of the SLD profile clearly shows how the Ag layer becomes thinner, how the Ch host layer changes, and how the interface layer grows. Time variation of the thickness of each layer is shown in Fig. 11. Similar to the result of the first peak position in the Fourier transform in Fig. 8, the Ag thickness rapidly decreases in the first 2 min and continues to decrease in the next 20 min, reaching a saturation for the Ag 50 nm/ $\text{Ge}_{40}\text{S}_{60}$ 200 nm/Si substrate, while the Ag thickness rapidly decreases in the first 10 min and continues to decrease slowly until the light shutter is closed for the Ag 50 nm/ $\text{Ge}_{40}\text{S}_{60}$ 150 nm/Si substrate. As for the time variation of the Ch host layer thickness, it is similar to that of the Ag thickness for Ag 50 nm/ $\text{Ge}_{40}\text{S}_{60}$ 200 nm/Si, while it is difficult to find changes for Ag 50 nm/ $\text{Ge}_{40}\text{S}_{60}$ 150 nm/Si because of the accuracy of the present analysis.

Time variation of the SLDs of the Ch host layer and the interface layer, causing a dip in the SLD depth profile, is shown in Fig. 12. For the Ag 50 nm/ $\text{Ge}_{40}\text{S}_{60}$ 200 nm/Si

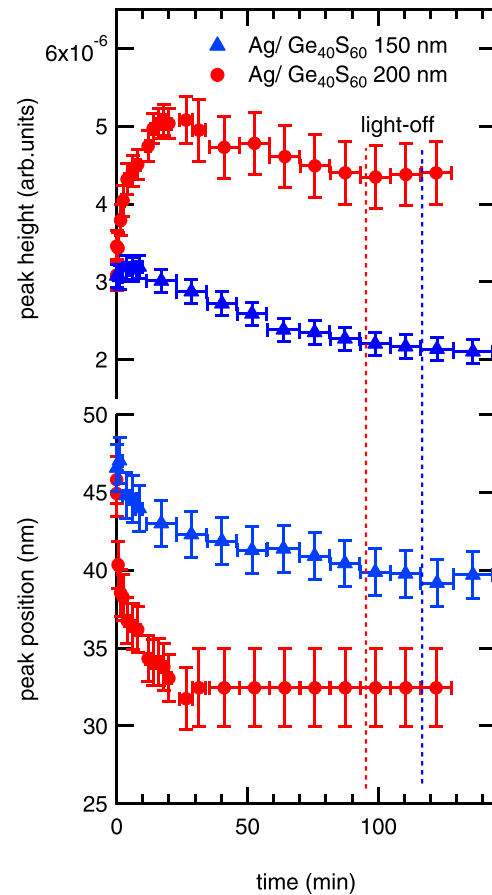


FIG. 8. Time variation of the position and the height of the first peak in the Fourier transform in Figs. 6 and 7. The result of Ag 50 nm/ $\text{Ge}_{40}\text{S}_{60}$ 150 nm/Si is indicated by blue triangles and that of Ag 50 nm/ $\text{Ge}_{40}\text{S}_{60}$ 200 nm/Si is indicated by red circles.

substrate, the SLD of the Ch host layer rapidly increases in the first 2 min and continues to increase in the next 20 min, reaching a saturation. For the Ag 50 nm/ $\text{Ge}_{40}\text{S}_{60}$ 150 nm/Si substrate, the SLD of the Ch host layer gradually increases in the first 10 min and continues to increase slowly until the light shutter is closed. This is consistent with the change in the Ag thickness, and the results are considered reasonable because the content of the missing Ag ions from the Ag layer should be equal to the increase in the Ag ions in the Ch host layer, leading to the increase in the SLD of the Ch host layer.

Time variations of the difference in the SLD between the Ag layer and the interface layer [ΔSLD (Ag/interface)], and the difference in the SLD between the Ch host layer and the interface layer [ΔSLD (Ch host/interface)] are shown in Fig. 13. As explained in Sec. III A 1, the height of the first peak in the Fourier transform is related to ΔSLD (Ag/interface). Therefore, time variations of the peak height and ΔSLD (Ag/interface) are supposed to show similar behavior. In fact, the time variation of ΔSLD (Ag/interface) (Fig. 13) is similar to that of the peak height (Fig. 8). The result can also support the SLD model, obtained from the fitting. The ΔSLD (Ch host/interface) indicates the depth of the interface layer; zero means no dip in the SLD profile. Time variation of ΔSLD (Ch host/interface) shows how the dip grows during the light exposure and how much remains after the light exposure. The dip of the Ag 50 nm/ $\text{Ge}_{40}\text{S}_{60}$ 200 nm/Si substrate is about

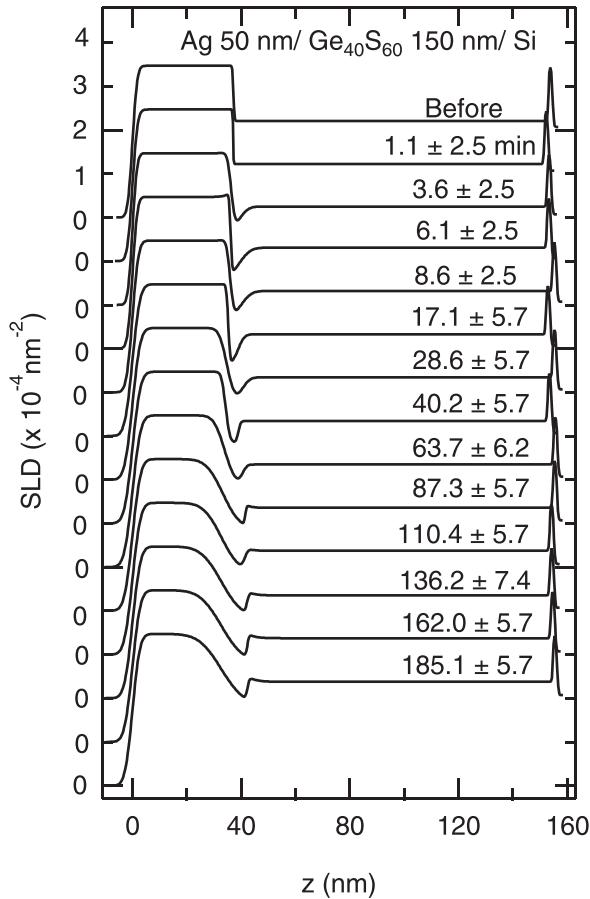


FIG. 9. Time evolution of the SLD profile of the Ag 50 nm/Ge₄₀S₆₀ 150 nm/Si substrate, obtained from the fitting to the neutron reflectivity curve in Fig. 4. The curves are shifted vertically for readability.

three times deeper than that of the Ag 50 nm/Ge₄₀S₆₀ 150 nm/Si substrate.

B. Mechanism of silver photodiffusion into Ge-rich Ge chalcogenide

1. Ag capturing site in Ge chalcogenide

It was found from the present study on Ge-rich Ge chalcogenide that the Ag layer was not exhausted by the prolonged light exposure for more than 90 min. On the other hand, in our previous study, we observed that the Ag layer was immediately dissolved into the Ch host layer exhausting the Ag layer with the thickness of 50 nm when the chalcogenide is Ge₂₀S₈₀ 150 nm.²⁵ The results suggest that more Ag ions are dissolved into the Ge-chalcogenide layer with more sulfur content. In addition, it was found from the present study and the previous study on Ge₃₃S₆₇/Ag that more Ag ions can dissolve into the thicker Ch layer.²⁹ Considering the compositional dependence and the Ch layer thickness dependence, the content of dissolved Ag ions seems to be determined by the content of sulfur atoms. This is consistent with the intercalation model, proposed by Kluge.⁴¹ According to the model, the intercalation of Ag ions occurs under participation of Ch-Ch and Ge-Ch bonds by which new Ch⁻Ag⁺ bonds are created. We infer that such capturing of Ag ions takes place in the vicinity of the Ag/Ch interface. Considering the immediate diffusion over the Ch host layer, the capture of Ag ions is supposed to be

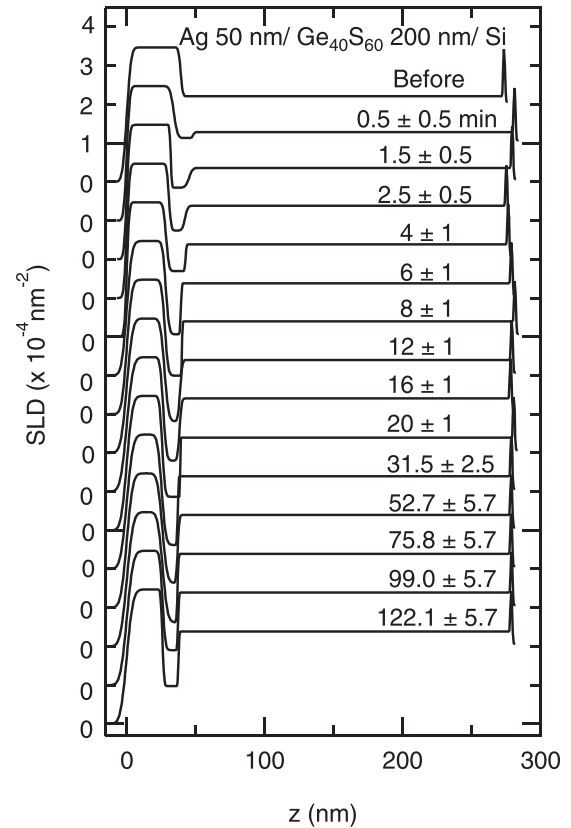


FIG. 10. Time evolution of the SLD profile of the Ag 50 nm/Ge₄₀S₆₀ 200 nm/Si substrate, obtained from the fitting to the neutron reflectivity curve in Fig. 5. The curves are shifted vertically for readability.

dynamic; the capturing site moves to other neighboring chalcogen sites. Presumably, such a local movement of the capturing site will lead to the silver diffusion in the whole layer.

From the neutron reflectivity measurement of Ag 50 nm/Ge₄₀S₆₀ 200 nm/Si, it was found that the thickness of the dissolved Ag layer was 13.5 nm and the thickness of the initial Ge₄₀S₆₀ layer was 234 nm. Assuming that all content of the dissolved Ag and the initial amount of the chalcogenide make one homogeneous compound and the mass density of Ge₄₀S₆₀ (Ref. 42) is 3.04 g/cm³, the compositional ratio of Ag to Ge_{0.4}S_{0.6} is estimated to be 8.9%. Also, from the neutron reflectivity measurement of Ag 50 nm/Ge₄₀S₆₀ 150 nm/Si, we obtained that the thickness of the dissolved Ag was 6 nm, and that the thickness of the initial chalcogenide layer was 116 nm. In this case, the compositional ratio of Ag to Ge_{0.4}S_{0.6} is estimated to be 8.0%. Time variation of Ag thickness in Fig. 11 shows that the light shutter was closed before reaching the saturation of Ag dissolution. Therefore, we expect that Ag can dissolve into the Ch host layer by 8.9% by more extended light exposure. In our previous study on the Ge₃₃S₆₇/Ag/Si substrate,²⁹ the saturated content of Ag was estimated to be 20% (Ag_{0.20}Ge_{0.27}S_{0.53}). Kawaguchi and Maruno¹⁰ also demonstrated that the total amount of photodoped Ag for Ag/Ge₃₃S₆₇ is about twice that of Ag/Ge₄₀S₆₀. We attribute the difference in the saturated amount of Ag to the difference in the structure of the host materials.⁴²⁻⁴⁶ The host amorphous materials are composed of several types of building blocks which form a network structure. According to Boolchand *et al.*,⁴⁴ amorphous Ge₃₃S₆₇ (GeS₂) consists of GeS₄ tetrahedral units and ethane-like S₃-Ge-Ge-S₃ clusters, which resulted from

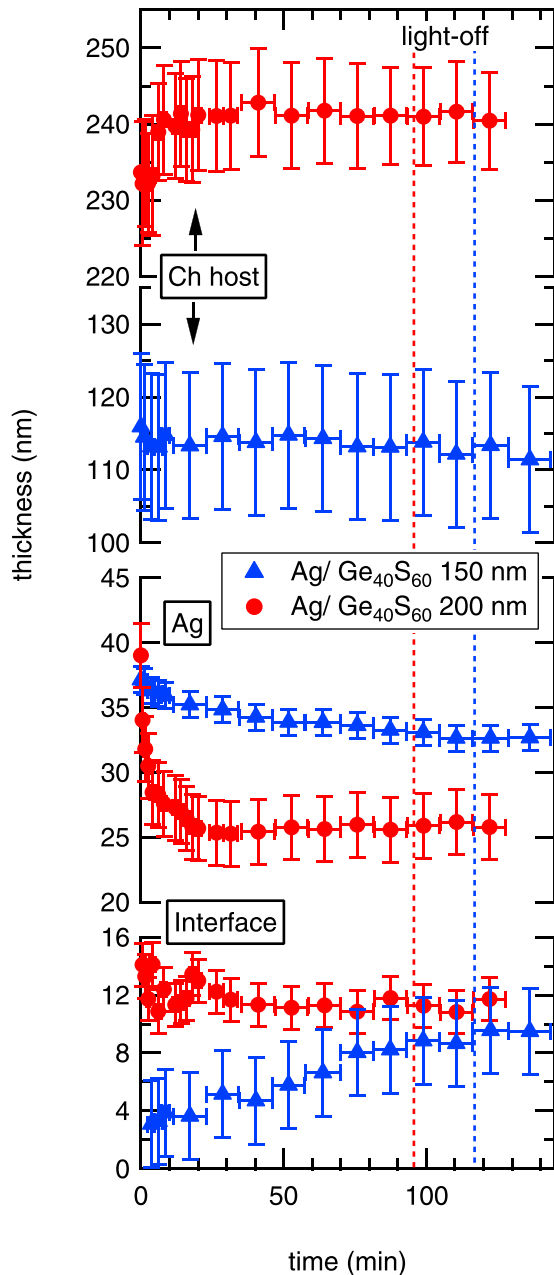


FIG. 11. Time variation of the thickness of the Ag layer, the Ch host layer, and the interface layer between the Ag layer and the Ch host layer. The result of Ag 50 nm/Ge₄₀S₆₀ 150 nm/Si is indicated by blue triangles and that of Ag 50 nm/Ge₄₀S₆₀ 200 nm/Si is indicated by red circles.

the broken chemical order in the amorphous phase, and amorphous Ge₄₀S₆₀ consists of ethane-like S₃-Ge-Ge-S₃ clusters and the fragments with a double-layer structure, which crystalline GeS has. In our previous work, we pointed out that the double layer is composed of zigzag GeS chains which alternatively align on two different planes.^{46,47} Such a difference in the building blocks must affect the saturated amount of Ag ions. Moreover, we assume that the structure of the host materials can also be related to the formation of a metastable Ag-rich reaction layer observed in the silver diffusion for S-rich Ge chalcogenide (Ge₂₀S₈₀ and Ge₂₅S₇₅). In the S-rich compound, there must have been S-S bonds available in the participation of Ag ions, in addition to Ge-S bonds in the GeS₄ tetrahedral unit. Such S-S bonds

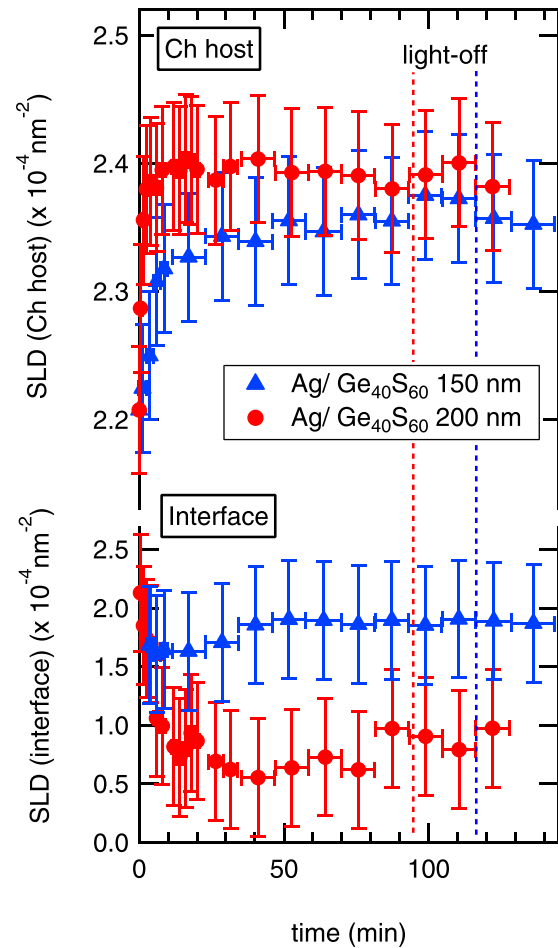


FIG. 12. Time variation of the SLD of the Ch host layer and the interface layer. The result of Ag 50 nm/Ge₄₀S₆₀ 150 nm/Si is indicated by blue triangles and that of Ag 50 nm/Ge₄₀S₆₀ 200 nm/Si is indicated by red circles.

will contribute to the production of a different type of reaction layer.

2. Photo-induced kinetics

A study on the reaction rate is also important to understand the mechanism of silver photodiffusion. So far, the time-dependence of the amount of Ag or reaction products was investigated by X-ray diffraction,¹⁵ optical measurement,^{10,11,13,22} RBS,¹⁸ and electrical resistivity.^{8,9} Basically, the reaction curve markedly depends on the Ch composition, and it would not be easy to describe a unified reaction process. However, Wagner *et al.*^{11,13,22} quantitatively discussed the reaction rate for Ag/As₃₃S₆₇ using the data on the modified reflectivity measurement. According to their results, there are two stages in silver photodiffusion. The thickness of the photo-diffused layer exponentially increases in the first stage, and the next second stage is described by a linear rate or a parabolic rate. In the present study, we plotted the thickness of the Ag layer, subtracted from the residual thickness after prolonged light exposure, on a semi-logarithmic plane as shown in Fig. 14. It seems that there are two exponential decay processes with a certain transition time at 10 min for Ag 50 nm/Ge₄₀S₆₀ 150 nm/Si and 2 min for Ag 50 nm/Ge₄₀S₆₀ 200 nm/Si. From curve fitting to a double-exponential form

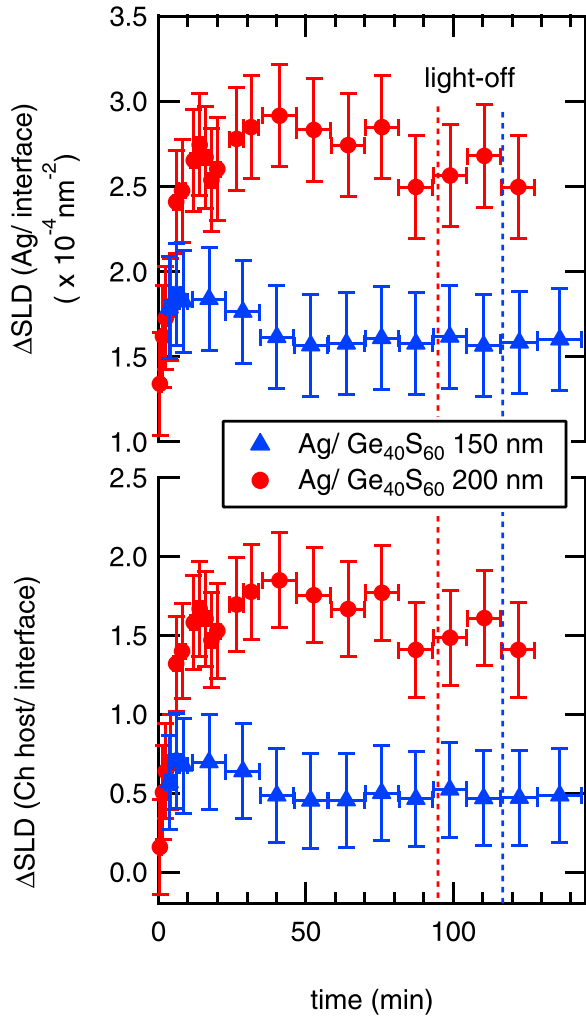


FIG. 13. Time variations of the difference in the SLD between the Ag layer and the interface layer (upper half) and the difference in the SLD between the Ch host layer and the interface layer (lower half). The result of Ag 50 nm/Ge₄₀S₆₀ 150 nm/Si is indicated by blue triangles and that of Ag 50 nm/Ge₄₀S₆₀ 200 nm/Si is indicated by red circles.

$$d_{Ag}(t) = A_1 \exp(-t/\tau_1) + A_2 \exp(-t/\tau_2), \quad (4)$$

we obtained $\tau_1 = 7.8$ min and $\tau_2 = 188.6$ min for Ag 50 nm/Ge₄₀S₆₀ 150 nm/Si and $\tau_1 = 0.6$ min and $\tau_2 = 9.2$ min for Ag 50 nm/Ge₄₀S₆₀ 200 nm/Si.

Considering the simple reaction $A + B \rightarrow P$ (A, B : reactant; P : product), the rate equation can be written as

$$\frac{d[A]}{dt} = -k[A][B], \quad (5)$$

where $[X]$ indicates the concentration of X and k is the reaction rate. The reaction rate, k , indicates the chance (or, the probability) of producing P from A and B , and is determined by the frequency of the collision between the reactants A and B . In the present experiment, there are two reactants; one is Ag and the other is the vacant Ag capturing chalcogen sites. However, in the vicinity of the interface, the concentration of Ag should always be 100%, because a bulky Ag layer always exists unless the Ag layer is consumed by silver diffusion. Therefore, the equation may be written in a simpler form:

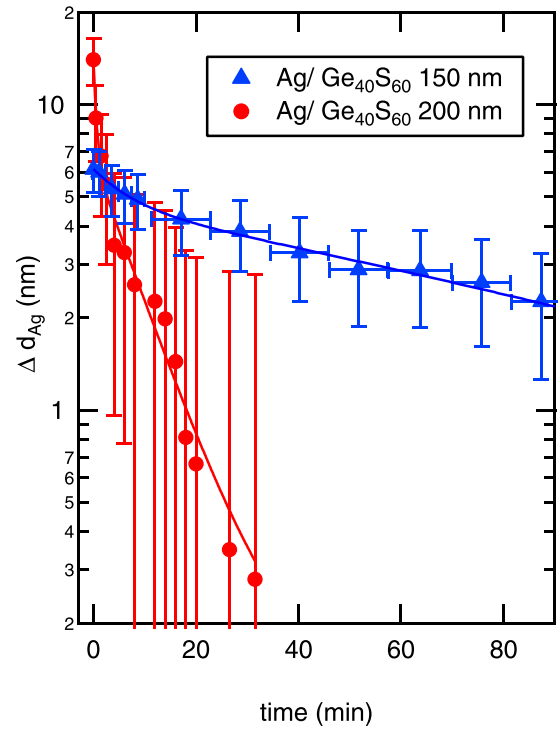


FIG. 14. Time variation of the thickness of the Ag layer, subtracted from the residual thickness after prolonged light exposure, in Ag 50 nm/Ge₄₀S₆₀ 150 nm/Si and Ag 50 nm/Ge₄₀S₆₀ 200 nm/Si.

$$\frac{d[A]}{dt} = -k[A]. \quad (6)$$

In this case, we obtain

$$[A] = [A]_0 \exp(-kt), \quad (7)$$

as the solution of $[A]$.⁴⁸ Between k and τ (relaxation time), there is a relationship

$$k = 1/\tau. \quad (8)$$

Considering the above equations, the double exponential form in Eq. (4) indicates that there are two types of vacant chalcogen sites with a different potential barrier to capture Ag ions. According to the *ab initio* simulations for Ag-Ge_xSe_{1-x}, it was shown that there were two types of Ag ions: most diffusive and less diffusive.⁴⁹ Such two types of Ag ion motions could be related to the two types of the vacant Ag capturing chalcogen sites. In addition, the presence of different types of building blocks could be related to the two types of vacant chalcogen sites as discussed in Sec. III B 1.

It is also noted that the relaxation time markedly depends on the Ch thickness. From the present study, it was found that the Ag ions diffused all over the Ch host layer immediately after starting the light exposure, forming a uniform layer. This means that the Ag capturing vacant sites also move. In other words, the vacant Ag capturing sites are successively supplied to the region in the vicinity of the interface from the Ch host layer, and the concentration is kept at a higher level unless the Ag capturing sites are exhausted in the Ch host layer. The thicker Ch layer can provide more available capturing sites, and it is good to remember that the actual Ch thickness in Ag 50 nm/Ge₄₀S₆₀

200 nm/Si (234 nm) is almost twice that in Ag 50 nm/Ge₄₀S₆₀ 150 nm/Si (116 nm), as shown in Fig. 3. The successive supply of the vacant Ag capturing sites will provide an additional chance for the collision between the reactants. Therefore, such a diffusion-driven accelerating factor, $k_{DF}(d)$ (>1), which depends on the Ch thickness, d , will be added to the original reaction rate, k_0 , resulting in a higher reaction rate

$$k = k_{DF}(d)k_0 > k_0 = 1/\tau_0. \quad (9)$$

For different thicknesses ($d_1 > d_2$)

$$k_{DF}(d_1)k_0 > k_{DF}(d_2)k_0. \quad (10)$$

Therefore

$$k_1 = k_{DF}(d_1)k_0 = 1/\tau_1 > k_2 = k_{DF}(d_2)k_0 = 1/\tau_2. \quad (11)$$

Thus

$$\tau_1 < \tau_2. \quad (12)$$

This would be the reason why the relaxation time markedly depends on the Ch thickness.

3. Origin of the interface layer

It was found from the present study that the interface layer, between the Ag layer and the Ch host layer, appears causing a dip in the SLD depth profile. It is noted that the value is considerably small, less than $1.0 \times 10^{-4} \text{ nm}^{-2}$. Obviously, this is not a reaction layer because the SLD of the reaction layer should be between 3.47 (Ag) and $2.21 (\text{Ge}_{40}\text{S}_{60}) \times 10^{-4} \text{ nm}^{-2}$. There could be two possibilities. One possibility is an actual less dense depth region, like a porous layer with a lot of voids inside. The other possibility is a region where specular reflection is partially lost from some reasons.

In fact, we observed the former case in Ge₃₃S₆₇/Ag/Si,²⁹ in which the surface layer was finally peeled off by the extended light exposure. A sort of vacant layer was observed in the neutron reflectivity measurement before the macroscopic change. The growth of the vacancy can be regarded as a precursor of the macroscopic detachment. In the present experiment, we did not observe such macroscopic detachment, and the Ag layer and the Ch host layer are supposed to contact to each other, because silver photodiffusion takes place. Considering the situation, this case would not be probable.

Although the situation is a little bit different, we observed a great loss of specular reflection when a visible macroscopic in-plane structure was formed on the surface of the Ge₄₀Se₆₀/Ag film after extended light exposure.²⁶ Similar to this case, we assume that a great loss of specular reflection can also appear when an in-plane inhomogeneous structure is formed on the Ag/Ch interface. Such an in-plane structure could be essentially related to the initial process of the Ag dissolution into the Ch layer. So far, Elliott⁵⁰ proposed an initial stage of silver photodiffusion, considering the growth of the nucleation in both the depth direction and the lateral one, from their SEM observation: (1) the formation of dendrites of a photo-induced reaction product originating from grain-boundary nucleation sites in the metal and (2) the subsequent lateral photodiffusion

between dendrites. Also, Murakami and Wakaki⁵¹ demonstrated by atomic force microscopy of GeS₂/Ag films that an inhomogeneous lateral structure appeared in the photodiffusion process, suggesting the nucleation of the channel of the silver-diffusion in the depth direction and the lateral growth of the channel. Probably, such nucleation sites may appear at the interface in the process of photodiffusion and the inhomogeneity on the plane may lead to a great loss of specular reflection from the interface region.

Comparing the two samples, Ag 50 nm/Ge₄₀S₆₀ 200 nm/Si has a deeper dip in the SLD profile. Considering the higher reaction rate in Ag 50 nm/Ge₄₀S₆₀ 200 nm/Si, the channel of the silver diffusion is supposed to grow greater and the loss in the specular reflection will be greater. This would be the reason why the dip is deeper in Ag 50 nm/Ge₄₀S₆₀ 200 nm/Si.

IV. CONCLUSIONS

We measured time-resolved neutron reflectivity of Ag/Ge₄₀S₆₀/Si to clarify the kinetics of silver photodiffusion into Ge-rich Ge chalcogenide. In contrast to S-rich Ge chalcogenide such as Ag/Ge₂₀S₈₀/Si, there is no metastable reaction layer between the Ag layer and the Ch host layer, and Ag ions immediately diffuse all over the Ch host layer once silver dissolves into the host layer. This behavior is the same as that of the stoichiometric composition, Ge₃₃S₆₇, and the formation of the metastable reaction layer could be the characteristic of the S-rich Ge chalcogenide. It was found from the decay curve that the Ag dissolution is determined by two types of Ag capturing chalcogen sites. The presence of two types of chalcogen sites must be related to the variety of structural units in the materials. Also, the observed relaxation time showed anomalous Ch thickness dependence. This is attributed to an additional diffusion-driven accelerating factor, which is unique to silver photodiffusion. Furthermore, we observed indicative changes of the formation of an inhomogeneous in-plane structure at the Ag/Ch host layer interface. This may be related to the nucleation and growth of the Ag-dissolved reaction product.

ACKNOWLEDGMENTS

The neutron reflectivity measurements were performed on a SHARAKU (BL17) in J-PARC MLF under Project No. 2012A0068. We would like to thank M. Ailavajhala (BSU) and Al Amin Ahmed Simon (BSU) for the sample preparation, and D. Yamazaki (JAEA), K. Soyama (JAEA), N. Miyata (CROSS), K. Akutsu (CROSS), T. Hanashima (CROSS), H. Aoki (JAEA) and S. Kasai (CROSS) for technical support for neutron reflectivity measurements. The X-ray diffraction and X-ray reflectivity measurements were performed at Nano-Processing Facility, National Institute of Advanced Industrial Science and Technology. We would like to thank K. Matsuno for technical support for the measurements.

APPENDIX A: X-RAY DIFFRACTION MEASUREMENTS

X-ray diffraction was measured for Ag 50 nm/Ge₄₀S₆₀ 150 nm/Si and Ag 50 nm/Ge₄₀S₆₀ 200 nm/Si, which were exposed to the light of the xenon lamp for the time-resolved

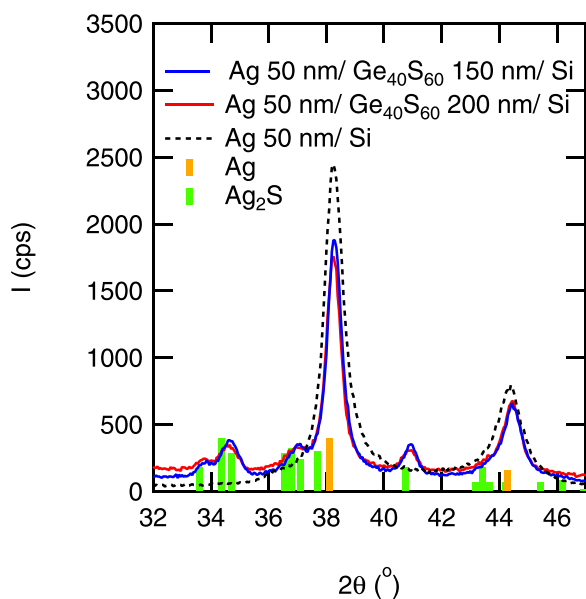


FIG. 15. X-ray diffraction profiles of Ag 50 nm/Ge₄₀S₆₀ 150 nm/Si and Ag 50 nm/Ge₄₀S₆₀ 200 nm/Si, which were exposed to the light of the xenon lamp for the time-resolved neutron reflectivity measurement.

neutron reflectivity measurement. The result is shown in Fig. 15. It is clear from the figure that the Ag layer remained even after the light exposure. The X-ray diffraction measurement was performed after five years of the neutron reflectivity

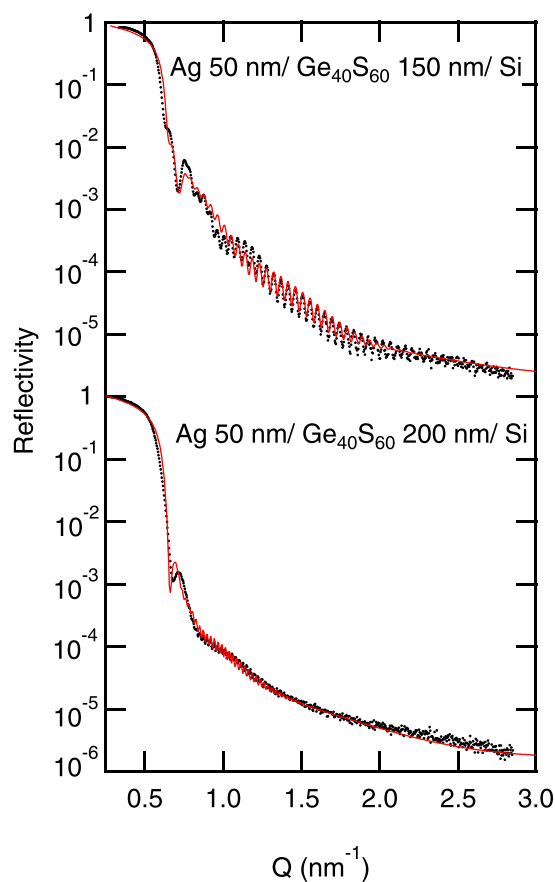


FIG. 16. X-ray reflectivity profiles of Ag 50 nm/Ge₄₀S₆₀ 150 nm/Si and Ag 50 nm/Ge₄₀S₆₀ 200 nm/Si, which were exposed to the light of the xenon lamp for the time-resolved neutron reflectivity measurement. The red curves indicate the calculated reflectivity curves obtained from model fitting.

measurement, and there could be some aging effects on the samples. There are other smaller peaks at 33.8°, 34.6°, 36.9°, and 40.9°. Those peaks can be assigned as the diffraction peaks of monoclinic Ag₂S, and Ag₂S could appear as a result of the aging effect.

APPENDIX B: X-RAY REFLECTIVITY MEASUREMENTS

X-ray reflectivity was measured for Ag 50 nm/Ge₄₀S₆₀ 150 nm/Si and Ag 50 nm/Ge₄₀S₆₀ 200 nm/Si, which were exposed to the light of the xenon lamp for the time-resolved neutron reflectivity measurement. The X-ray reflectivity profiles are shown in Fig. 16 and the SLD profiles are shown in Fig. 17. Figure 18 shows Fourier transforms of RQ^4 for the reflectivities in Fig. 16. The measurement was also performed after five years of the neutron reflectivity measurement. However, the basic structure in the SLD profile is the same as that obtained from the neutron reflectivity measurement (Fig. 3), and the layer structure is considered to be maintained. The thicknesses of the Ag and Ge₄₀S₆₀ layers are almost the same between the SLD profiles obtained from X-ray reflectivity and neutron reflectivity. This can also be confirmed by the result of Fourier transform in Figs. 18 and 2. The presence of the interface layer with a dip in the SLD profile was confirmed from both X-ray reflectivity (Fig. 17) and neutron reflectivity (Fig. 3).

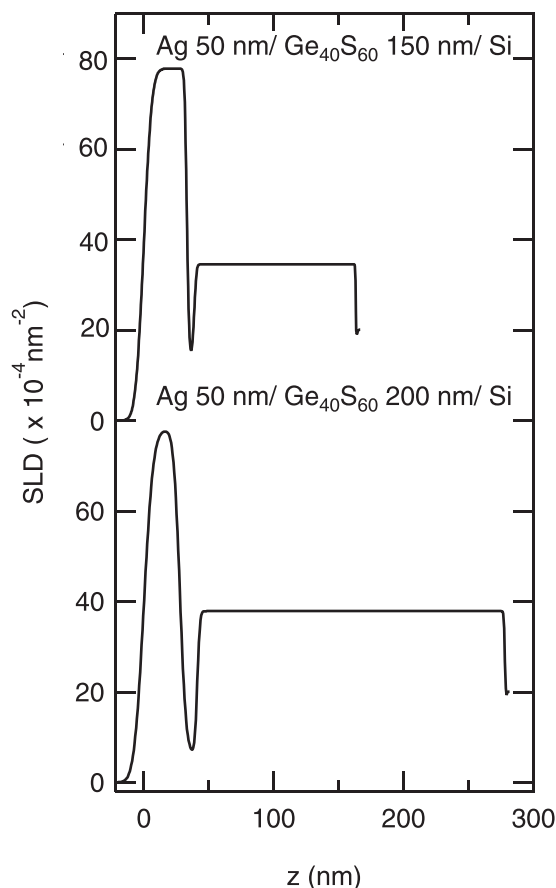


FIG. 17. The SLD profiles obtained from the fitting to the X-ray reflectivity curves in Fig. 16.

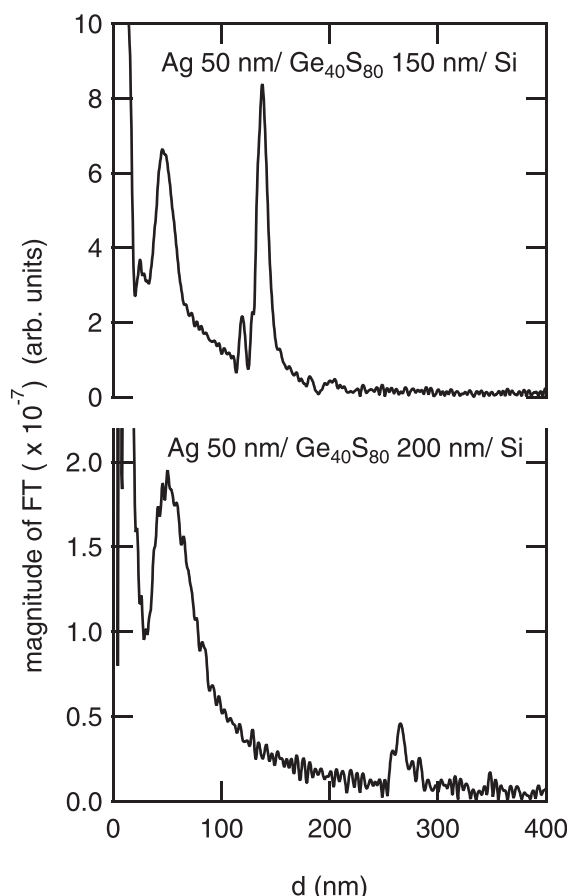


FIG. 18. Fourier transforms of RQ^4 for the reflectivities in Fig. 16. The Q range for the Fourier transform was selected to obtain comparatively sharp peaks.

¹Photo-Induced Metastability in Amorphous Semiconductors, edited by A. V. Kolobov (Wiley-VCH, Weinheim, 2003).
²M. T. Kostyshin, E. V. Mikhailovskaya, and P. F. Romanenko, *Sov. Phys. (Solid State)* **8**, 451 (1966).
³A. V. Kolobov and S. R. Elliott, *Adv. Phys.* **40**, 625 (1991).
⁴A. Yoshikawa, O. Ochi, H. Nagai, and Y. Mizushima, *Appl. Phys. Lett.* **29**, 677 (1976).
⁵J. Hajto, P. J. S. Ewen, R. E. Belford, and A. E. Owen, *Thin Solid Films* **200**, 229 (1991).
⁶Y. Murakami, K. Arai, M. Wakaki, T. Shibuya, and T. Shintaku, *Proc. SPIE* **9359**, 93591N (2015).
⁷M. Mitkova and M. N. Kozicki, *J. Non-Cryst. Solids* **299–302**, 1023 (2002).
⁸D. Goldschmidt and P. S. Rudman, *J. Non-Cryst. Solids* **22**, 229 (1976).
⁹D. Goldschmidt, T. Bernstein, and P. S. Rudman, *Phys. Status Solidi A* **41**, 283 (1977).
¹⁰T. Kawaguchi and S. Maruno, *J. Appl. Phys.* **71**, 2195 (1992).
¹¹T. Wagner, M. Vlcek, V. Smrcka, P. J. S. Ewen, and A. E. Owen, *J. Non-Cryst. Solids* **164–166**, 1255 (1993).
¹²T. Wagner, M. Vlcek, K. Nejezchleb, M. Frumar, V. Zima, V. Perina, and P. J. S. Ewen, *J. Non-Cryst. Solids* **198–200**, 744 (1996).
¹³T. Wagner, E. Marquez, J. Fernandez-Pena, J. M. Gonzalez-Leal, P. J. S. Ewen, and S. O. Kasap, *Philos. Mag. B* **79**, 223 (1999).
¹⁴J. H. S. Rennie and S. R. Elliott, *J. Non-Cryst. Solids* **77–78**, 1161 (1985).
¹⁵T. Wagner and M. Frumar, *J. Non-Cryst. Solids* **116**, 269 (1990).
¹⁶Y. Yamamoto, T. Itoh, Y. Hirose, and H. Hirose, *J. Appl. Phys.* **47**, 3603 (1976).
¹⁷J. Rennie, S. R. Elliott, and C. Jeynes, *Appl. Phys. Lett.* **48**, 1430 (1986).
¹⁸G. Kluge, A. Thomas, R. Klages, R. Grotzschel, and P. Suptitz, *J. Non-Cryst. Solids* **124**, 186 (1990).

¹⁹R. E. Grandi, J. Calas, G. Galibert, and M. Averous, *Thin Solid Films* **218**, 259 (1992).
²⁰J. Calas, R. E. Grandi, G. Galibert, and A. Traverse, *Nucl. Instrum. Methods Phys. Res. B* **63**, 462 (1992).
²¹T. Wagner, V. Perina, M. Vlcek, M. Frumer, E. Rauhala, J. Saarihahti, and P. J. S. Ewen, *J. Non-Cryst. Solids* **212**, 157 (1997).
²²T. Wagner, G. Dale, P. J. S. Ewen, E. Owen, and V. Perina, *J. Appl. Phys.* **87**, 7758 (2000).
²³R. Klages, A. Thomas, G. Kluge, W. Beyer, R. Grotzschel, and P. Suptitz, *Phys. Status Solidi A* **106**, 57 (1988).
²⁴A. Kovalskiy, A. C. Miller, H. Jain, and M. Mitkova, *J. Am. Ceram. Soc.* **91**, 760 (2007).
²⁵Y. Sakaguchi, H. Asaoka, Y. Uozumi, Y. Kawakita, T. Ito, M. Kubota, D. Yamazaki, S. K. M. Ailavajhala, M. R. Latif, and M. Mitkova, *Can. J. Phys.* **92**, 654 (2014).
²⁶Y. Sakaguchi, H. Asaoka, Y. Uozumi, Y. Kawakita, T. Ito, M. Kubota, D. Yamazaki, K. Soyama, M. Ailavajhala, M. R. Latif, K. Wolf, M. Mitkova, and W. A. Skoda, *J. Phys.: Conf. Ser.* **619**, 012046 (2015).
²⁷Y. Sakaguchi, H. Asaoka, Y. Uozumi, Y. Kawakita, T. Ito, M. Kubota, D. Yamazaki, K. Soyama, M. Ailavajhala, K. Wolf, M. Mitkova, and M. W. A. Skoda, *JPS Conf. Proc.* **8**, 031023 (2015).
²⁸Y. Sakaguchi, H. Asaoka, Y. Uozumi, Y. Kawakita, T. Ito, M. Kubota, D. Yamazaki, K. Soyama, G. Sheoran, and M. Mitkova, *Phys. Status Solidi A* **213**, 1894 (2016).
²⁹Y. Sakaguchi, H. Asaoka, Y. Uozumi, K. Kondo, D. Yamazaki, K. Soyama, M. Ailavajhala, and M. Mitkova, *J. Appl. Phys.* **120**, 055103 (2016).
³⁰*X-ray and Neutron Reflectivity: Principles and Applications*, Lecture Notes in Physics, edited by J. Daillant and A. Gibaud (Springer, Berlin, Heidelberg, 2009), p. 770.
³¹J. Als-Nielsen and D. McMorrow, *Elements of Modern X-Ray Physics*, 2nd ed. (Wiley, 2011).
³²D. S. Silvia, *Elementary Scattering Theory for X-Ray and Neutron Users* (Oxford University Press, Oxford, 2011).
³³F. Bridou, J. Gautier, F. Delmotte, M.-F. Ravet, O. Durand, and M. Modreanu, *Appl. Surf. Sci.* **253**, 12 (2006).
³⁴K. Sakurai, M. Mizusawa, and M. Ishii, *Trans. Mater. Res. Soc. Jpn.* **33**, 523 (2008).
³⁵M. Takeda, D. Yamazaki, K. Soyama, R. Maruyama, H. Hayashida, H. Asaoka, T. Yamazaki, M. Kubota, K. Aizawa, M. Arai, Y. Inamura, T. Itoh, K. Kaneko, T. Nakamura, T. Nakatani, K. Oikawa, T. Ohhara, Y. Sakaguchi, K. Sakasai, T. Shinohara, J. Suzuki, K. Suzuya, I. Tamura, K. Toh, H. Yamagishi, N. Yoshida, and T. Hirano, *Chin. J. Phys.* **50**, 161 (2012).
³⁶A. Nelson, *J. Appl. Crystallogr.* **39**, 273 (2006).
³⁷M. Mitkova, M. N. Kozicki, H. C. Kim, and T. L. Alford, *Thin Solid Films* **449**, 248 (2004).
³⁸M. Mitkova, M. N. Kozicki, H. C. Kim, and T. L. Alford, *J. Non-Cryst. Solids* **338–340**, 552 (2004).
³⁹M. Mitkova, Y. Wang, and P. Boolchand, *Phys. Rev. Lett.* **83**, 3848 (1999).
⁴⁰M. Mitkova, Y. Sakaguchi, D. Tenne, S. K. Bhagat, and T. L. Alford, *Phys. Status Solidi A* **207**, 621 (2010).
⁴¹G. Kluge, *Phys. Status Solidi A* **101**, 105 (1987).
⁴²H. Takebe, H. Maeda, and K. Morinaga, *J. Non-Cryst. Solids* **291**, 14 (2001).
⁴³G. Lucovsky, F. L. Galeener, R. C. Keezer, R. H. Geils, and H. A. Six, *Phys. Rev. B* **10**, 5134 (1974).
⁴⁴P. Boolchand, J. Grothaus, M. Tenhover, M. A. Hazle, and R. K. Grasselli, *Phys. Rev. B* **33**, 5421 (1986).
⁴⁵P. Boolchand, X. Feng, and W. J. Bresser, *J. Non-Cryst. Solids* **293–295**, 348 (2001).
⁴⁶Y. Sakaguchi, D. A. Tenne, and M. Mitkova, *J. Non-Cryst. Solids* **355**, 1792 (2009).
⁴⁷Y. Sakaguchi, D. A. Tenne, and M. Mitkova, *Phys. Status Solidi B* **246**, 1813 (2009).
⁴⁸P. W. Atkins, *Physical Chemistry* (Oxford University Press, Oxford, 1998).
⁴⁹D. N. Tafen, D. A. Drabold, and M. Mitkova, *Phys. Rev. B* **72**, 054206 (2005).
⁵⁰S. R. Elliott, *J. Non-Cryst. Solids* **130**, 85 (1991).
⁵¹Y. Murakami and M. Wakaki, *Thin Solid Films* **542**, 246 (2013).